Title	Ferromagnetic amorphous oxides in the EuO-TiO[2] system studied by the Faraday effect in the visible region and the x-ray magnetic circular dichroism at the Eu M[4,5] and L[2,3] edges
Author(s)	Kawamoto, Takahiro; Fujita, Koji; Akamatsu, Hirofumi; Nakamura, Tetsuya; Kinoshita, Toyohiko; Mizumaki, Masaichiro; Kawamura, Naomi; Suzuki, Motohiro; Kususe, Yoshiro; Murai, Shunsuke; Tanaka, Katsuhisa
Citation	Physical Review B (2013), 88(2)
Issue Date	2013-07-08
URL	http://hdl.handle.net/2433/188014
Right	©2013 American Physical Society
Type	Journal Article
Textversion	publisher

Ferromagnetic amorphous oxides in the EuO-TiO_2 system studied by the Faraday effect in the visible region and the x-ray magnetic circular dichroism at the Eu $M_{4,5}$ and $L_{2,3}$ edges

Takahiro Kawamoto,[1] Koji Fujita,[1,*] Hirofumi Akamatsu,[1] Tetsuya Nakamura,[2] Toyohiko Kinoshita,[2] Masaichiro Mizumaki,[2] Naomi Kawamura,[2] Motohiro Suzuki,[2] Yoshiro Kususe,[1] Shunsuke Murai,[1] and Katsuhisa Tanaka[1]

[1]*Department of Material Chemistry, Graduate School of Engineering, Kyoto University, Nishikyo-ku, Kyoto 615-8510, Japan*

[2]*Japan Synchrotron Radiation Research Institute, SPring-8, 1-1-1 Kouto, Sayo-cho, Sayo-gun, Hyogo 679-5198, Japan*

(Received 18 December 2012; revised manuscript received 1 May 2013; published 8 July 2013)

Amorphous Eu_2TiO_4 and $EuTiO_3$ have been studied by a combination of the Faraday effect in the visible region and polarization-dependent x-ray absorption spectroscopy at the Eu $M_{4,5}$ and $L_{2,3}$ edges to examine the role of Eu $4f$-$5d$ exchange interactions on the ferromagnetic behavior. The bulk-sensitive x-ray absorption spectra (XAS) for Eu $L_{2,3}$ edges show that most of the europium ions are present as the divalent state in the amorphous Eu_2TiO_4 and $EuTiO_3$. The Eu $M_{4,5}$ edge x-ray magnetic circular dichroism (XMCD) signals, measured for the amorphous Eu_2TiO_4, dramatically increase upon cooling through the Curie temperature (16 K) determined by a superconducting quantum interference device (SQUID) magnetometer. Sum-rule analysis of the XMCD at Eu $M_{4,5}$ edges measured at 10 K yields a $4f$ spin magnetic moment of $6.6\mu_B$ per Eu^{2+} ion. These results confirm that the ferromagnetic properties exclusively arise from $4f$ spins of Eu^{2+}. In addition, for both the amorphous Eu_2TiO_4 and $EuTiO_3$, the temperature and magnetic-field dependence of Eu $L_{2,3}$ edge XMCD signals can be scaled with the corresponding magnetization measured by SQUID, indicating that the $5d$ magnetic polarization of Eu^{2+} is involved in the process to cause the ferromagnetic interaction between Eu^{2+} ions. We further discuss the origin of ferromagnetism in the amorphous system on the basis of the energy diagram of Eu $4f$ and $5d$ levels deduced from the Faraday effect in the visible region. From the wavelength dependence of Faraday rotation angles of the amorphous EuO-TiO_2 system in comparison with those of the divalent Eu chalcogenides as reported previously, it is found that the magnitude of crystal-field splitting of Eu $5d$ levels in the former is on the same order as that in the latter, which explains an enhanced ferromagnetic exchange interaction between Eu $4f$ and $5d$ states.

DOI: 10.1103/PhysRevB.88.024405 PACS number(s): 78.20.Ls, 75.50.Kj, 75.50.Dd

I. INTRODUCTION

In amorphous magnetic oxides, where the magnetic cations are randomly distributed in the three-dimensional disordered network, short-range antiferromagnetic superexchange interactions via the O $2p$ states, based on the Kramers-Anderson mechanism, are predominant as demonstrated by the fact that negative values of Weiss temperature have been reported for most of the oxide glasses.[1–8] The random distribution of the magnetic ions and the prevailing antiferromagnetic superexchange interaction among the magnetic ions inevitably cause geometrical frustrations in the ordering of the magnetic moments, leading to spin-glass transitions at low temperatures.[1–8] Consequently, oxide glasses containing a high concentration of magnetic ions are typical of insulating spin-glass systems where long-range interactions such as Ruderman-Kittel-Kasuya-Yoshida interactions are not at work.

An exception to this general trend is Eu^{2+}-containing oxide glasses, which are insulating but have the ferromagnetic interactions as signified by the positive Weiss temperatures.[9–12] Recently, we have confirmed the existence of a definite ferromagnetic state in amorphous EuO-TiO_2 system.[10,11] The amorphous $EuTiO_3$ (a-ETO) shows a ferromagnetic transition at the Curie temperature (T_C) of 5.5 K, although its crystalline form, i.e., $EuTiO_3$ with perovskite-type structure, is an antiferromagnet with the Néel temperature (T_N) of 5.3 K.[13,14] This is a rare example of an insulating magnetic oxide that shows amorphization-induced ferromagnetism. Also, amorphous Eu_2TiO_4 (a-2ETO) exhibits a ferromagnetic transition at $T_C = 14$ K,[11] while $T_C = 9$ K for its crystalline form, or Eu_2TiO_4 with K_2NiF_4-type structure.[15] Interestingly, the T_C values of a-ETO and a-2ETO are comparable to or higher than the magnetic transition temperatures of their crystalline counterparts, respectively. The amorphization-induced enhancement of ferromagnetic interaction is less common and thus clarification of local structure and electronic structure in the amorphous phases is of importance to understand the nature of magnetic interaction between Eu^{2+} ions in compounds including oxides, sulfides, selenide, and so on.

Recent x-ray absorption fine structure studies revealed that the local structure of Eu^{2+} in a-ETO and a-2ETO is similar to that in EuO with rock-salt-type structure rather than their crystalline counterparts.[16] Such a local environment of Eu^{2+} is known to be closely related to the magnitude of an indirect ferromagnetic exchange interaction often observed in Eu^{2+}-based oxides, which involves an Eu $4f$ electron excited to the Eu $5d$ band where it interplays with another Eu $4f$ spin on the neighboring Eu^{2+} ion.[17,18] The coupling constant of the indirect exchange interaction is proportional to $J_{intra}b^2/U_{fd}^2$, where J_{intra} is the intra-atomic exchange constant between the Eu $4f$ and $5d$ states, b is the transfer integral between the neighboring Eu ions, and U_{fd} is the energy difference between the Eu $4f$ and $5d$ levels. The U_{fd} value becomes smaller with an increase in the crystal-field splitting of the Eu $5d$ levels, resulting in the enhancement of the ferromagnetic indirect exchange interaction. The $5d$ crystal-field splitting of a-ETO, which we assume from the local structural analysis we have done so far, is schematically illustrated in Fig. 1 along with those of rock-salt-type EuO and perovskite-type

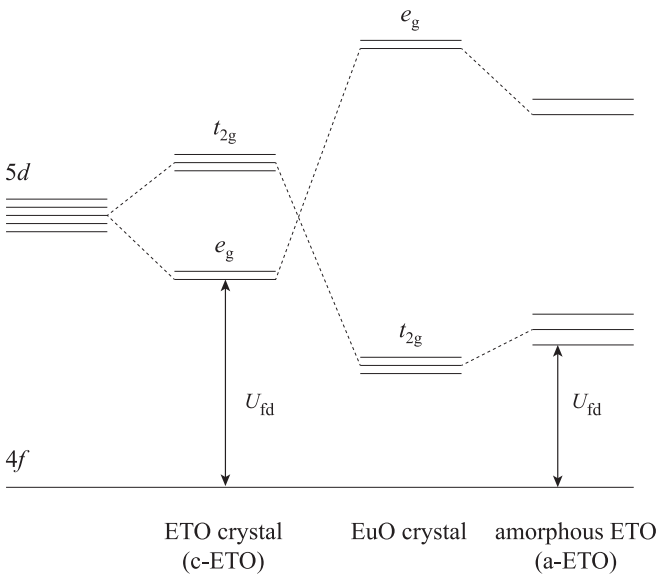

FIG. 1. Schematic energy diagram of the 5d and 4f states for Eu^{2+} in $EuTiO_3$ crystal (c-ETO), EuO crystal, and amorphous $EuTiO_3$ (a-ETO) (from left to right). The 5d crystal-field splitting is drawn based on the energy level scheme described in Refs. 14 and 16. The larger crystal-field splitting for a-ETO compared to c-ETO results in the smaller energy separation between the 4f levels and the lower levels of 5d states.

$EuTiO_3$ crystals.[14] The 5d crystal-field splitting is much larger in EuO crystal than in $EuTiO_3$ crystal, which accounts for the much stronger indirect exchange interactions in the former that is a ferromagnet with $T_C = 69$ K.[19] Given the similarity in local environment of Eu^{2+} between a-ETO and EuO crystal, the 5d crystal-field splitting in the former is considered to be of the same order as that in the latter. As a result, it is expected that the 5d crystal-field splitting is larger in the amorphous system than in the crystalline counterpart, with the ferromagnetic indirect exchange coupling being more favorable in the former. Although this energy diagram is in agreement with the occurrence of amorphization-induced ferromagnetism, the crystal-field splitting of Eu 5d states in the amorphous system has not been experimentally elucidated so far.

In order to shed light on the crystal-field splitting of Eu 5d states of the amorphous EuO-TiO_2 system, we have here investigated the Faraday effect in the visible region, which is ascribable to the Eu 4f to 5d electronic transitions. We also present the temperature (T) and magnetic-field (H) dependence of the Eu 4f and 5d magnetizations using the x-ray magnetic circular dichroism (XMCD) at Eu $M_{4,5}$ and $L_{2,3}$ edges to examine the contributions of Eu 4f and 5d states to the ferromagnetic transition in the system. Polarization-dependent x-ray absorption spectroscopy is a powerful tool for determining the element origin of magnetism in magnetic materials.[20–29] Since the x-ray absorption spectra (XAS) at $M_{4,5}$ edges are associated with excitation of electrons from Eu 3d to 4f states, the corresponding XMCD directly probes magnetization of the 4f shell of Eu. On the other hand, the XAS at $L_{2,3}$ edges arises from transitions from Eu 2p to 5d and hence the XMCD at the Eu $L_{2,3}$ edge probes the Eu 5d magnetization. The appearance of the XMCD signal at the Eu $L_{2,3}$ edge is expected when there is an ordered Eu 5d moment due to the Eu 4f-5d exchange. The results of Faraday effect measurements qualitatively support the energy diagram in Fig. 1, and the results of XMCD measurements are in good agreement with the scenario that the amorphization-induced ferromagnetism is caused by the ferromagnetic Eu 4f-5d exchange interaction.

II. EXPERIMENTAL DETAILS AND SAMPLE CHARACTERISTICS

In our previous report, we prepared a-ETO and a-2ETO thin films on SiO_2 glass substrates by a pulsed laser deposition (PLD) method.[10,11] In a typical procedure, a KrF excimer laser with a wavelength of 248 nm, a repetition frequency of 10 Hz, and a fluence of 2 J/cm^2 was focused on the $EuTiO_3$ and Eu_2TiO_4 ceramic targets under an ultrahigh vacuum condition of about 10^{-6} Pa. Deposition of thin films was performed without intentional heating of substrates. Structural characterization, including x-ray diffraction, transmission electron microscope observation, Rutherford backscattering spectroscopy and ^{151}Eu conversion-electron Mössbauer spectroscopy revealed that our previous samples were formed without precipitation of any crystalline phases or phase separation and that the Eu/Ti ratio in the thin films was very close to those in the target compositions, with more than 90% of europium ions being present as the divalent oxidation state.[10,11] For the present work, samples of a-ETO and a-2ETO thin films were prepared not only on SiO_2 glass substrates (0.5 mm thickness) but also on Kapton foils (12 μm thickness) under the same deposition condition as described in Refs. 10 and 11. First, we examined the influence of substrates on macroscopic magnetic behavior using a superconducting quantum interference device (SQUID) magnetometer (MPMS-XL; Quantum Design). Figure 2 shows the temperature dependence of magnetization, $M(T)$, of a-ETO and a-2ETO thin films deposited on Kapton foils, measured at $H = 100$ Oe applied parallel to the sample surface. Both zero-field-cooling and field-cooling processes were performed. For both thin films, the $M(T)$ curve shows a steep increase upon cooling, signifying the paramagnetic-ferromagnetic transition. The T_C value, defined as an inflection point in the $M(T)$ curve, is 6.0 K for a-ETO [Fig. 2(a)] and 15 K for a-2ETO [Fig. 2(b)], in agreement with the values of our previous samples deposited on the SiO_2 glass substrates.[10,11] Also, no detectable difference in macroscopic magnetic behavior was observed between samples newly prepared on the SiO_2 substrates and Kapton foils. Next, we checked the magnetic anisotropy of the thin films. Figure 3 shows the magnetic-field dependence of magnetization, $M(H)$, obtained at 2 K for the a-2ETO thin film deposited on the SiO_2 glass substrate. H was applied up to 5 T along the directions parallel (in plane) and perpendicular (out of plane) to the sample surface. The in-plane $M(H)$ curve exhibits a steep increase at very low H. The saturation magnetization is about 7μ_B/Eu, which coincides with the full moment of Eu^{2+} ($S = 7/2$). On the other hand, the out-of-plane $M(H)$ curve tends to be saturated at higher H (>4 T). After being corrected for the demagnetizing field effect, the magnetization behavior was observed to follow the

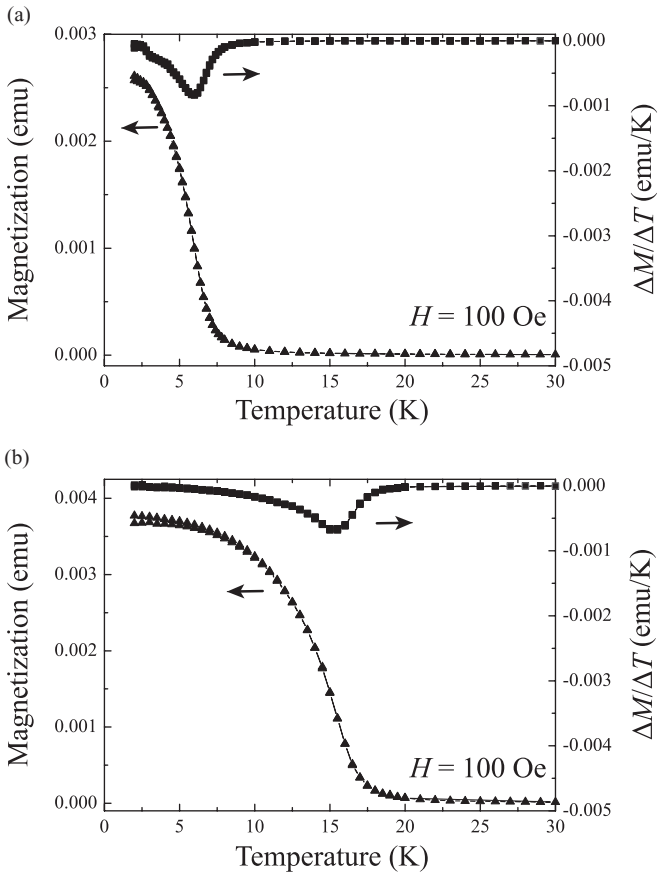

FIG. 2. Temperature dependence of magnetization of a-ETO (a) and a-2ETO thin films (b) deposited on Kapton foils (triangles), measured at an external magnetic field (H) of 100 Oe using SQUID magnetometer. From temperature derivative of magnetization curves, $\Delta M/\Delta T$ (squares), the Curie temperature is determined to be 6.0 K for a-ETO and 15 K for a-2ETO, in agreement with those of our previous samples deposited on SiO_2 glass substrates, as described in Ref. 11.

in-plane $M(H)$ curve. Namely, the present amorphous system can be regarded as being magnetically isotropic.

To verify the energy scheme of Eu $4f$ and $5d$ levels as depicted in Fig. 1, we measured the room-temperature optical absorption and paramagnetic Faraday effect in the visible region for a-ETO and a-2ETO thin films deposited on SiO_2 glass substrates. The optical absorption spectra were recorded by using a spectrophotometer (JASCO, V-570). The wavelength dependence of Faraday rotation angles was obtained with a commercial measurement system (JASCO, Model K-250) using an Xe lamp as a light source. In the measurement, the light beam was directed perpendicularly to the sample surface and the magnetic field of $H = 15$ kOe was applied along the direction of the light beam. The Faraday rotation angle of the thin film was estimated by subtracting the diamagnetic contribution of the SiO_2 glass substrate.

Polarization-dependent x-ray absorption spectroscopy was carried out for the newly prepared thin-film samples. For the soft-x-ray experiments at the Eu $M_{4,5}$ edges, the 100-nm-thick thin films deposited on SiO_2 glass substrates were terminated with a 3-nm-thick Au cap layer to protect the thin-film surface from oxidation; after the thin film was formed by the PLD

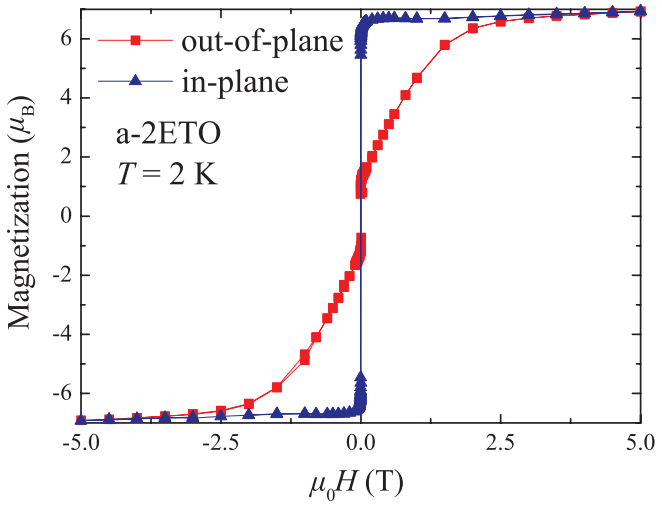

FIG. 3. (Color online) Magnetic-field dependence of magnetization of a-2ETO thin film deposited on SiO_2 glass substrate, measured at 2 K using SQUID magnetometer. The magnetic field (H) is applied along the directions parallel (in plane) and perpendicular (out of plane) to the sample surface.

method, an Au cap layer was deposited in the same PLD chamber without being exposed to the atmosphere. As for the hard-x-ray experiment at the Eu $L_{2,3}$ edges, Kapton foils served as substrates because they permitted measurements in the transmission mode. Ten pieces of Kapton foils, on which the 100-nm-thick thin films were deposited, were stacked to obtain the optimized XAS intensity of the L_3 absorption-edge jump of Eu. The XAS and XMCD at Eu $M_{4,5}$ and $L_{2,3}$ edges were measured at the soft-x-ray beamline BL25SU and hard-x-ray beamline BL39XU of SPring-8, respectively. In both the soft- and hard-x-ray experiments, the x-ray beam, with a high degree of circular polarization ($P_C \geqslant 95\%$), was incident perpendicularly to the sample surface, and H was applied along the x-ray beam direction; an electromagnet ($H \leqslant 1.9$ T) and a split-type superconducting magnet ($H \leqslant 5$ T) were utilized for the experiments at Eu $M_{4,5}$ and $L_{2,3}$ edges, respectively.[30] The total electron yield (TEY) method was employed to acquire the XAS and XMCD at the Eu $M_{4,5}$ edges,[30] whereas the XAS and XMCD at the Eu $L_{2,3}$ edges were recorded in the transmission mode using the helicity-modulation technique.[31] XMCD was given by the difference of x-ray absorption coefficients for the right- (μ^+) and left- (μ^-) circular polarizations, $\Delta\mu(E) = (\mu^+ - \mu^-)$, and XAS was obtained as $\mu(E) = (\mu^+ + \mu^-)/2$. The nonmagnetic background was removed by combining the XMCD signals for parallel and antiparallel directions of H relative to the x-ray beam direction.

III. RESULTS

A. Room-temperature Faraday effect in the visible region

Figure 4(a) shows the optical absorption spectra of 100-nm-thick a-ETO and a-2ETO thin films at room temperature. Each of the thin-film samples exhibits an absorption band centered at around the wavelength of $\lambda = 410$ nm. We observed a large Faraday effect in the vicinity of the absorption edge at

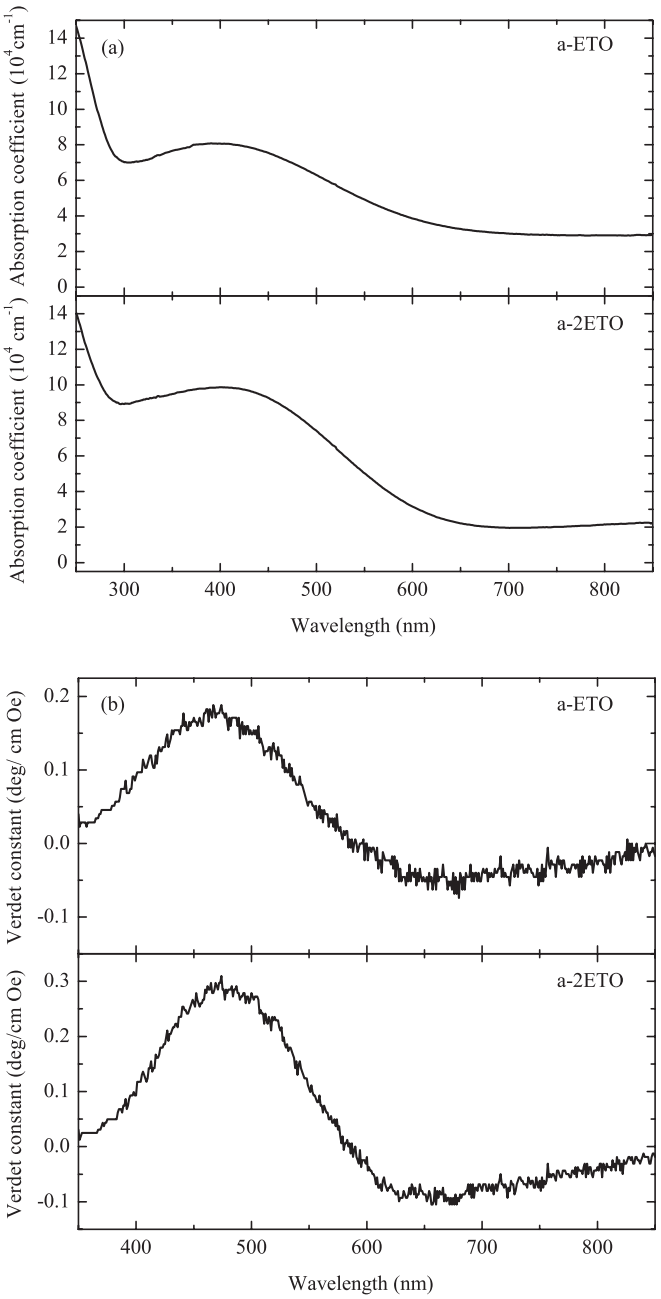

FIG. 4. (a) Room-temperature optical absorption spectra in the visible region for 100-nm-thick a-ETO and a-2ETO thin films. (b) Wavelength dependence of the Verdet constant at room temperature for a-ETO and a-2ETO.

around $\lambda = 600$ nm. The magnitude of the Faraday effect is evaluated by the Verdet constant, $V = \theta/(Hl)$, where θ is the Faraday rotation angle, H is the magnetic field, and l is the thin-film thickness. The wavelength dependence of the Verdet constant, $V(\lambda)$, is displayed for a-ETO and a-2ETO in Fig. 4(b). One can see that $V(\lambda)$ shows a maximum at around 470 nm and a minimum near 660 nm, and the sign in V changes at approximately 600 nm corresponding to the absorption edge. The observed behavior of $V(\lambda)$ is quite different from those for bulk Eu^{2+}-containing oxide glasses as reported previously, which are characterized by negative values of $V(\lambda)$ decreasing monotonically with decreasing λ.[32–35] Rather, $V(\lambda)$ for the amorphous EuO-TiO_2 system resembles in shape those for the thin films of divalent europium chalcogenides of rock-salt type, such as EuO,[36,37] EuS,[38–40] and EuSe[41] [in some case, the shape of $V(\lambda)$ of the divalent Eu chalcogenides was assumed from the magnetic circular dichroism through Kramers-Kronig conversion[42]]. In the case of divalent Eu chalcogenides (EuX; X = Se, S, O), the optical absorption peak ascribed to the $4f^7 \rightarrow 4f^6 5d$ (t_{2g}) transition appears in the visible to near-infrared region.[18] The absorption edge corresponding to the onset of optical absorption is located near the wavelengths of 670 nm (X = Se),[41] 750 nm (X = S),[38,40] and 900 nm (X = O)[36] at room temperature, and $V(\lambda)$ shows a maximum and a minimum with its sign changing at around the corresponding absorption edge. By comparing the present data with those for EuX compounds, we found that the maximum and minimum positions in $V(\lambda)$ for a-ETO and a-2ETO are very similar to those for EuSe thin film; for the latter, the maximum and minimum in $V(\lambda)$ are located at 500 and 600 nm, respectively.[41] In addition, the magnitude of V for the amorphous system is as large as 0.2 deg/Oe cm at 500 nm and -0.08 deg/Oe cm at 660 nm, comparable to those obtained for EuSe thin film (0.36 deg/Oe cm at 500 nm and -0.2 deg/Oe cm at 600 nm).[41] The correspondence in these aspects implies that the amorphous EuO-TiO_2 system (as well as the EuX compounds) has the large crystal-field splitting of Eu $5d$ states and hence the small energy separation between Eu $4f$ and $5d$ states (see Fig. 1), which causes the large Faraday effect due to the $4f^7 \rightarrow 4f^6 5d$ transition in the visible region. As mentioned above, the small $4f$-$5d$ energy difference U_{fd} should contribute to the enhancement of the ferromagnetic indirect exchange coupling.

B. XMCD at Eu $L_{2,3}$ edges

Figure 5 displays the XAS and XMCD at Eu $L_{2,3}$ edges of a-ETO and a-2ETO measured at $T = 1.9$ K and $H = 1.9$ T. Each of the Eu $L_{2,3}$ edge XAS [Figs. 5(a) and 5(c)] is characterized by an intense peak and a satellite structure, with an energy separation of ~10 eV; for example, the major peak and satellite for the Eu L_3 edge are observed at 6972 and 6981 eV, respectively, as indicated by the vertical dashed lines. According to our previous Eu L_3 edge XAS study,[16] the major peak and satellite are attributable to the contributions from Eu^{2+} and Eu^{3+} ions, respectively. To estimate the relative contributions of Eu^{2+} and Eu^{3+}, the XAS for Eu L_3 edge was deconvoluted by the superposition of two Lorentzians and two arctangent functions, according to the procedure used by Godart *et al.*[43] for the analysis of mixed valence in rare-earth intermediate compounds. In this procedure, the fit was constrained to have the same threshold energy for the XAS peak and step function for a given valence state. The result for a-2ETO is shown in Fig. 6, which shows that the spectral contribution from Eu^{2+} and Eu^{3+} ions is 98% and 2%, respectively. Similar analysis for a-ETO gave the spectral contribution of 97% from Eu^{2+} and 3% from Eu^{3+}. These results indicate that almost all the Eu ions are present as the divalent state in the present amorphous oxides, consistent with the result obtained by conversion-electron ^{151}Eu Mössbauer spectroscopy.[10,11] On the other hand, the Eu $L_{2,3}$ edge XMCD appears at 6973 and 7610 eV [Figs. 5(b) and 5(d)],

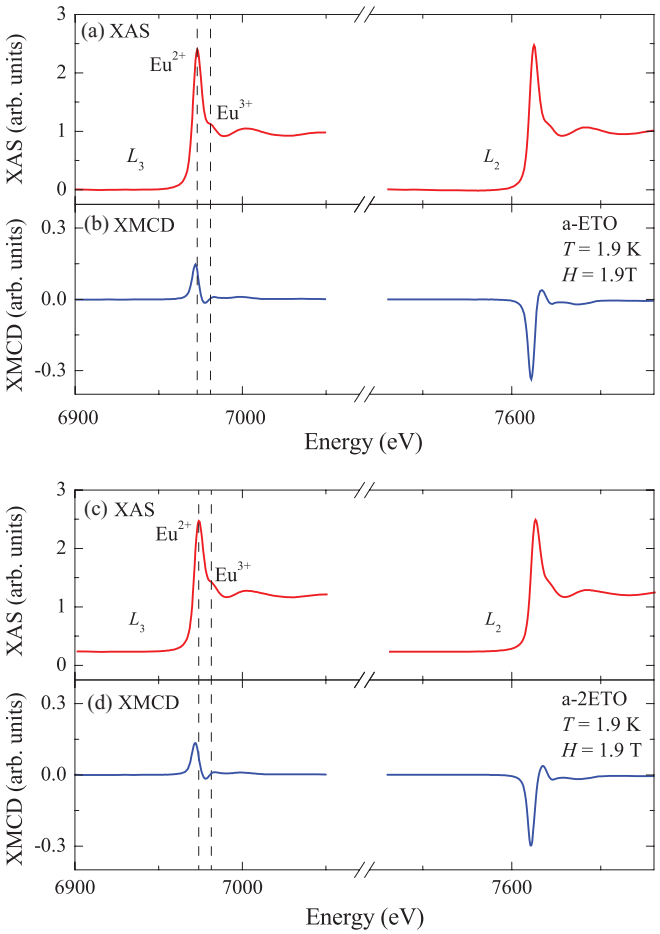

FIG. 5. (Color online) Eu $L_{2,3}$ edge XAS (a) and XMCD (b) of a-ETO thin film and Eu $L_{2,3}$ edge XAS (c) and XMCD (d) of a-2ETO thin film, measured at 1.9 K under an external magnetic field (H) of 1.9 T. The positions of the major peak and satellite for the Eu L_3 edge XAS are indicated by the vertical dashed lines.

corresponding to the edge energies determined from the maximum of the derivative of XAS. This fact confirms that the magnetism originates significantly from Eu^{2+} rather than Eu^{3+} in a-ETO and a-2ETO, although this is naturally imagined. Recalling that the XMCD at Eu $L_{2,3}$ edges provides information about the magnetic polarization of Eu $5d$ states,

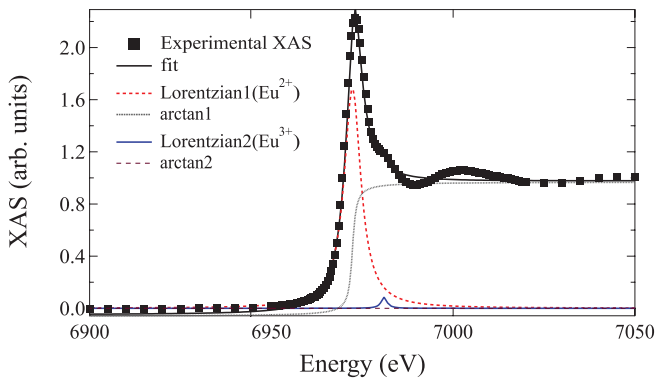

FIG. 6. (Color online) Fit of Eu L_3 edge XAS of a-2ETO thin film with the superposition of two Lorentzians and two arctangent functions.

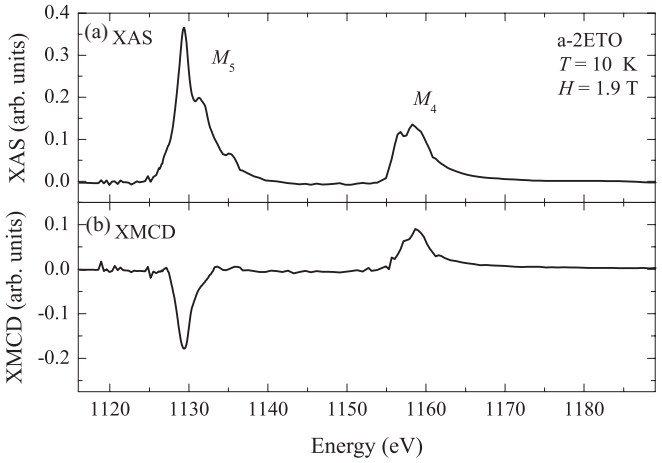

FIG. 7. Eu $M_{4,5}$ edge XAS (a) and XMCD (b) of a-2ETO thin film, measured at 10 K under an external magnetic field of 1.9 T.

the observation of XMCD signals implies the presence of the Eu $4f$-$5d$ exchange interactions. We can also see from Figs. 5(b) and 5(d) that the amplitude of XMCD signals for a-ETO is comparable to that for a-2ETO, indicating that the Eu $5d$ states in the former are magnetically polarized to the same extent as those in the latter. The origin of ferromagnetism in the amorphous EuO-TiO_2 system will be discussed later.

C. XMCD at Eu $M_{4,5}$ edges

Figures 7(a) and 7(b) show the XAS and XMCD at Eu $M_{4,5}$ edges for a-2ETO measured at $T = 10$ K under $H = 1.9$ T. Several peaks associated with the multiplet structures of Eu^{2+} and Eu^{3+} ions are observed in the XAS at both the M_5 and M_4 edges. The positions of the multiplet peaks match quite well with the theoretical positions for Eu^{2+} and Eu^{3+} ions as reported previously.[22,23] We have thus analyzed the experimental XAS with a linear combination of the theoretical XAS for Eu^{2+} and Eu^{3+} ions as displayed in Fig. 8(b), which was calculated using an atomic model with spherical symmetry.[23] The best fit to the experimental data, as shown in Fig. 8(a), yields the spectral contributions of 70% from Eu^{2+} and 30% from Eu^{3+} ions. The spectral contribution from Eu^{3+} in XAS is much larger for the Eu $M_{4,5}$ edge than for the Eu $L_{2,3}$ edge, because the surface oxidation of Eu^{2+} is preferentially detected due to the smaller probing depth for the soft x ray utilized (~5 nm in the TEY mode). Similar behavior was reported for mixed-valence Eu compounds.[25] Nevertheless, the Eu $M_{4,5}$ edge XMCD signals as depicted in Fig. 7 appear dominantly at the energies where the multiplet peaks due to Eu^{2+} are present in the XAS. We also analyzed the experimental XMCD for Eu $M_{4,5}$ edges with the theoretical XMCD of Eu^{2+} and Eu^{3+} as reported previously[26,29] (not shown), and confirmed a significant spectral contribution of magnetic Eu^{2+}, with a small portion of XMCD arising from the Van Vleck paramagnetism of Eu^{3+} due to the admixture of low-lying excited states.

According to the sum rules,[44,45] we determine the spin and orbital magnetic moments of the Eu^{2+} $4f$ shell from the observed XAS and XMCD. For the Eu $M_{4,5}$ edges, the orbital and spin angular momentum $\langle L_z \rangle$ and $\langle S_z \rangle$, respectively, can

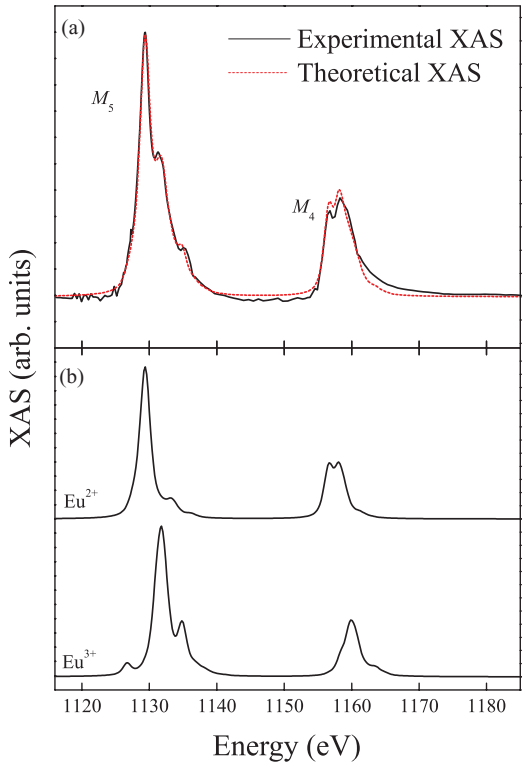

FIG. 8. (Color online) (a) Experimental XAS at the Eu $M_{4,5}$ edges for the a-2ETO thin film (solid curve) and the weighted sum of the theoretical XAS for Eu^{2+} and Eu^{3+} (broken curve). The experimental data were recorded at 10 K under an external magnetic field of 1.9 T. (b) Theoretical XAS of Eu^{2+} and Eu^{3+} obtained by atomistic multiplet calculations.

be expressed as

$$\langle L_z \rangle = -\frac{2N_{4f}\,(A_{M5} + A_{M4})}{I},$$

and

$$\langle S_z \rangle + 3\,\langle T_z \rangle = \frac{N_{4f}(2A_{M5} - 3A_{M4})}{2I},$$

where $A_{M5} = \int_{M_5} \Delta\mu\,(E)\,dE$ and $A_{M4} = \int_{M_4} \Delta\mu\,(E)\,dE$ are the integrated areas of XMCD at the M_5 and M_4 edges, respectively, N_{4f} is the number of holes in the Eu $4f$ shell, I is the sum of the integrated XAS intensity at M_5 and M_4 edges, that is, $I = \int_{M_4+M_5} \mu\,(E)\,dE$, and $\langle T_z \rangle$ is the magnetic-dipole operator for Eu. The $\langle T_z \rangle$ term was neglected in the present amorphous system because the magnetic-dipole interaction is isotropic. In the present analysis, we used the A_{M5}, A_{M4}, and I values for the Eu^{2+} components deduced from the observed XAS and XMCD at $M_{4,5}$ edge. The orbital and spin magnetic moments of Eu ions are given by $\mu_{\rm orb} = -\langle L_z \rangle \mu_B$ and $\mu_{\rm spin} = -2\,\langle S_z \rangle \mu_B$, respectively. Assuming $N_{4f} = 7$, the sum-rule analysis yields $\mu_{\rm spin} = 6.6\mu_{\rm B}$ per Eu^{2+} ion. The slightly small $\mu_{\rm spin}$ value compared to the theoretical spin moment ($S = 7/2$) is primarily caused by the fact that the out-of-plane $M(H)$ curve is not fully saturated at 1.9 T as demonstrated in Fig. 3. The orbital magnetic moment is deduced as $\mu_{\rm orb} = 0.19\mu_{\rm B}$ for Eu^{2+} ion using the sum rule, but the very small $\mu_{\rm orb}$ value may be within possible errors in the present analysis as compared with the theoretical orbital moment ($L = 0$).

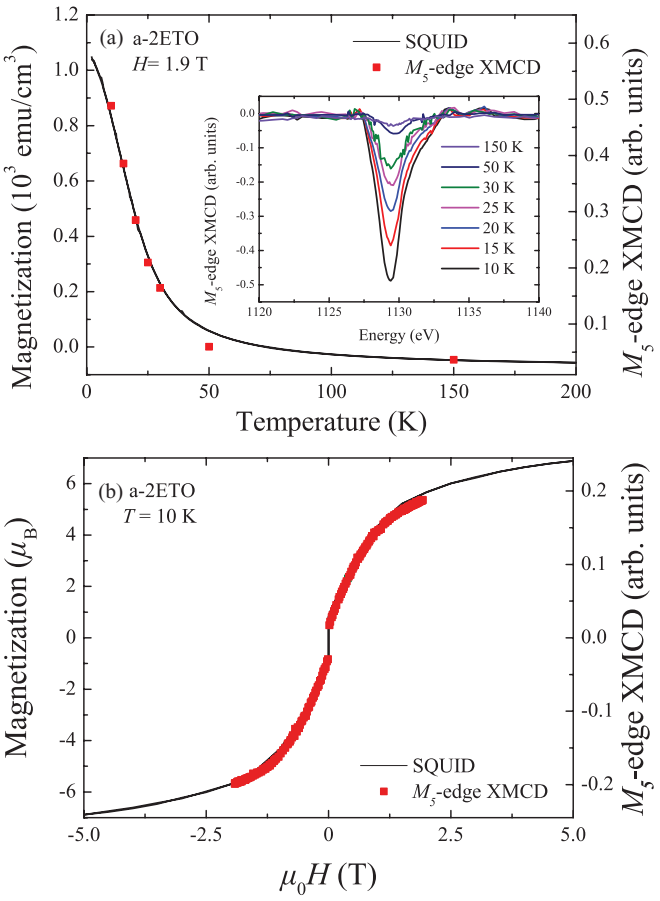

FIG. 9. (Color online) (a) Temperature dependences of the Eu M_5 edge XMCD signal amplitude (squares) and SQUID magnetization data (solid line), measured for a-2ETO under an external magnetic field (H) of 1.9 T applied perpendicular to the surface. Inset shows the Eu M_5 edge XMCD signals for the same sample at various temperatures between 15 and 150 K. (b) H dependences of the Eu $M_{4,5}$ edge XMCD signals (squares) and SQUID magnetization data (solid line), measured for a-2ETO at 10 K. The XMCD signals are plotted with the sign reversed.

D. A comparison between XMCD and SQUID data

Figure 9(a) shows the T dependence of M_5 edge XMCD signal measured for a-2ETO under $H = 1.9$ T. In the figure, the $M(T)$ curve of the thin-film sample determined by SQUID is also displayed for comparison. The XMCD signal starts to increase steeply as the sample is cooled below 50 K, and manifests a rapid increase at around $T_{\rm C}$ of 14 K [see also the inset of Fig. 9(a)]. Due to the application of the relatively high H, the magnetic transition becomes less clear, with the XMCD signals being induced in the temperature region where the sample is paramagnetic. It is found that the T dependence of XMCD signal is coincident with the $M(T)$ curve measured by SQUID. Figure 9(b) depicts the H dependence of the XMCD signal at 10 K, in comparison with the $M(H)$ curve obtained by SQUID. The XMCD and SQUID data exhibit a very similar

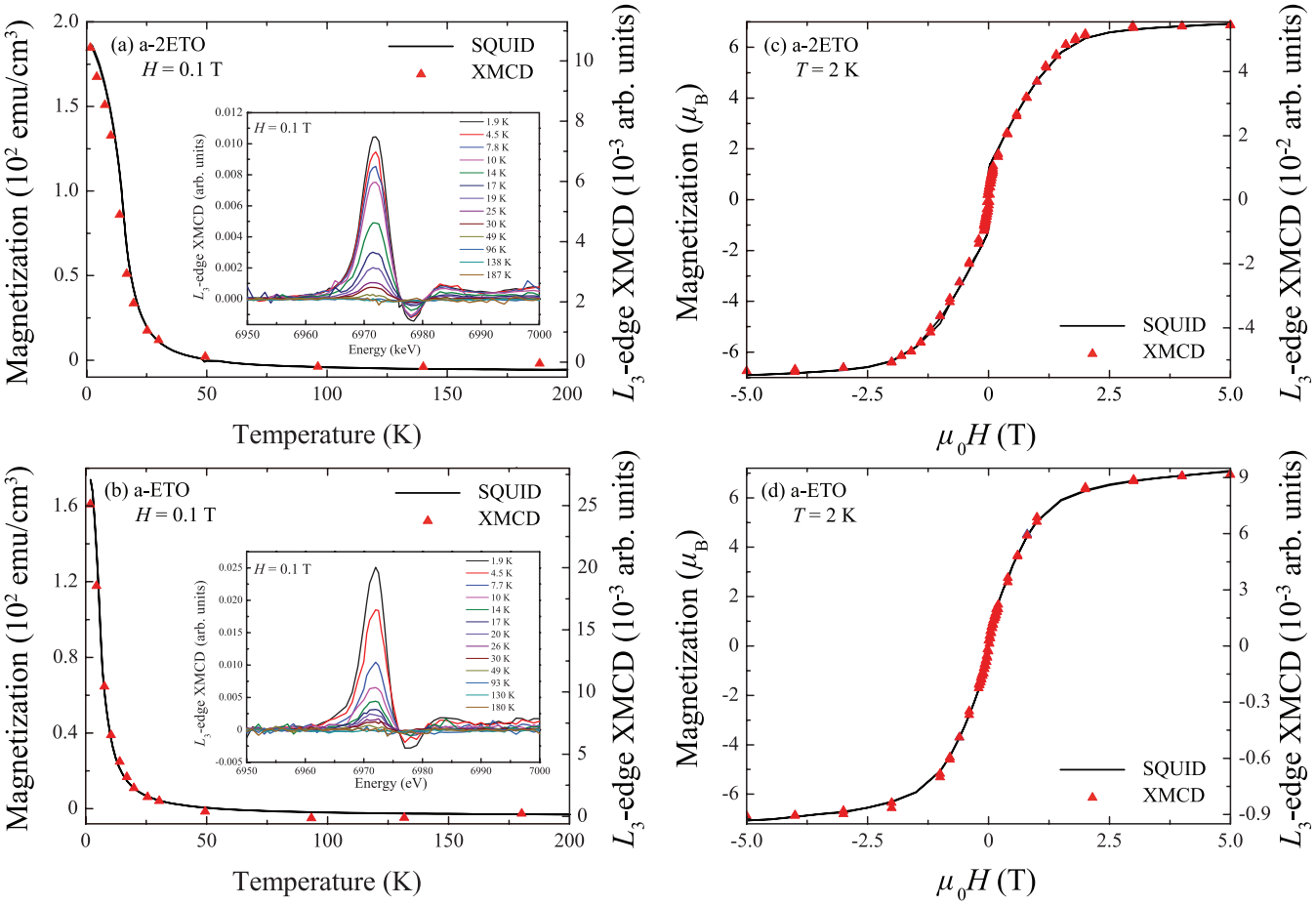

FIG. 10. (Color online) (a), (b) Temperature dependences of the Eu L_3 edge XMCD signals (triangles) and SQUID magnetization data (solid line), measured for the a-2ETO (a) and a-ETO (b) under an external magnetic field (H) of 0.1 T applied perpendicularly to the surface. The respective inset shows the Eu L_3 edge XMCD signals recorded at various temperatures between 1.9 and 187 K. (c), (d) H dependences of the Eu L_3 edge XMCD signals (triangles) and SQUID magnetization data (solid line), measured for a-2ETO (c) and a-ETO (d) at 2 K.

trend. These results confirm the ferromagnetic alignment of Eu $4f$ spins at low temperatures.

A scaling relation of XMCD signals to the magnetization data of the whole thin-film samples is observed at the Eu $L_{2,3}$ edges as well. Figure 10(a) compares the T dependence of the Eu L_3 edge XMCD signal and SQUID magnetization measured for a-2ETO under $H = 0.1$ T. As T is lowered below $T_C = 14$ K, the evolution of XMCD signals becomes pronounced [see also the inset of Fig. 10(a)], showing that the magnetic polarization of the Eu $5d$ states becomes more significant at lower temperatures. A similar behavior is observed when a-ETO is cooled below $T_C = 6$ K, as shown in Fig. 10(b). As depicted in Figs. 10(c) and 10(d), the H dependence of the Eu L_3 edge XMCD signals at 2 K for both a-2ETO and a-ETO also scales with the corresponding SQUID magnetization data. These observations clearly indicate that the ferromagnetic alignment of $4f$ spins of Eu^{2+} is mediated by the $5d$ magnetic polarization.

IV. DISCUSSION

Before discussing the ferromagnetic behavior of the amorphous oxides in the EuO-TiO_2 system, it is important to comment on the validity of the energy level scheme as shown in Fig. 1. As mentioned in Sec. III A, a-ETO and a-2ETO as well as EuX compounds (X = Se, S, O) exhibit a large Faraday effect attributable to the $4f^7 \rightarrow 4f^6 5d$ transition of Eu^{2+} in the visible region, and $V(\lambda)$ for the amorphous system resembles in shape those for the EuX compounds. In particular, $V(\lambda)$ for the amorphous system, as shown in Fig. 4, is very similar in both magnitude and shape to that for EuSe. In the EuX compounds of rock-salt type, the $5d$ levels of Eu^{2+} are split by the octahedral crystal field into a lower-energy t_{2g} triplet and a higher-energy e_g doublet, and the crystal-field splitting increases in the order that Se < S < O, corresponding to a decrease in lattice constant.[18] From these results, we assume that the $4f$-$5d$ energy difference for the amorphous system is comparable to the $4f$-$5d$ (t_{2g}) energy difference for EuSe, while it is slightly larger compared to that for EuO (see Fig. 1). In crystalline $EuTiO_3$, on the other hand, Eu^{2+} ions are present at the 12-fold-coordinated cuboctahedral sites and the $5d$ levels are split into a lower-energy e_g doublet and a higher-energy t_{2g} triplet. As Chien *et al.*[14] argued previously, the $5d$ crystal-field splitting for $EuTiO_3$ crystal is about one order of magnitude smaller than those for the EuX compounds.

Thus, it is reasonable to consider that the $4f$-$5d$ energy separation for the amorphous system is much smaller than that for the crystalline counterpart (see Fig. 1). This idea is in agreement with the fact that the amorphization of $EuTiO_3$ crystal results in a decrease in the coordination number of Eu^{2+} (12 in perovskite $EuTiO_3$ vs about 6 in a-ETO) as demonstrated by our previous analysis of x-ray absorption fine structure.[16] Namely, the reduction of coordination number of Eu^{2+} upon amorphization makes the crystal field acting on Eu^{2+} stronger in the amorphous phase than in the crystalline counterpart, resulting in the smaller $4f$-$5d$ energy separation for the former.

In the remainder of this section, we discuss the origin of amorphization-induced enhancement of ferromagnetic interaction in the EuO-TiO_2 system. The XMCD results for the Eu $M_{4,5}$ edges show that the ferromagnetic behavior of a-ETO and a-2ETO is not ascribable to the extrinsic factor such as the presence of ferromagnetic impurities but to the intrinsic one originating from the magnetic moment of the Eu $4f$ shell. In addition, the XMCD for the Eu $L_{2,3}$ edges confirms the presence of the magnetic polarization of the Eu $5d$ states, which is in agreement with the presence of the Eu $4f$-$5d$ exchange interaction. Two possible mechanisms have been proposed for the ferromagnetic interactions. One is the indirect exchange mechanism involving Eu $4f$ to $5d$ hopping and exchange, and the other is the superexchange mechanism, which is based on a cyclic process involving O $2p$ to Eu $5d$, Eu $4f$ to O $2p$, and Eu $5d$ to $4f$ hopping and Eu $4f$-$5d$ exchange.[17,18] Both of the ferromagnetic exchange mechanisms involve an exchange interaction between the Eu $4f$ and $5d$ states, depending on the energy separation between them. As discussed above, the amorphization of crystalline compounds in the EuO-TiO_2 system brings about the smaller $4f$-$5d$ energy separation. This variation of electronic structure should result in the enhancement of Eu $4f$-$5d$ interaction. Indeed, the ferromagnetic interaction is stronger in the amorphous phases than in the crystalline counterparts, as exemplified by the increase in Weiss temperature from 3.8 K for $EuTiO_3$ crystal to 8.0 K for a-ETO.[11] Thus, the overall structural and spectroscopic considerations strongly corroborate our idea that the Eu $4f$-$5d$ exchange interactions are responsible for the ferromagnetism in the amorphous EuO-TiO_2 system.

V. CONCLUSIONS

We have examined the Eu $M_{4,5}$ and $L_{2,3}$ edge XAS and XMCD of a-2ETO and a-ETO for which the macroscopic magnetic behavior was well characterized by a SQUID magnetometer. The analysis of Eu $L_{2,3}$ edge XAS demonstrates that the valence state of europium ions in a-2ETO and a-ETO is dominantly $+2$. The temperature and magnetic-field dependence of Eu $M_{4,5}$ edge XMCD signals exhibits ferromagnetic properties, consistent with SQUID magnetization data, and the sum-rule analysis shows that $\mu_{spin} = 6.6\mu_B$ per Eu, very close to the theoretical value expected from $S = 7/2$. The crucial result of the present work is that the Eu $L_{2,3}$ edge, as well as the $M_{4,5}$ edge XMCD signals, are pronounced upon cooling into the ferromagnetic state, indicating that the ferromagnetic ordering of the $4f$ electrons results from their intra-atomic exchange coupling with the magnetically polarized $5d$ electrons. The wavelength dependence of Faraday rotation angles in the visible region reveals that the crystal-field splitting of Eu $5d$ orbitals for the amorphous EuO-TiO_2 system is as large as those for divalent Eu chalcogenides, leading to the small $4f$-$5d$ energy separation that causes the electronic transition in the visible region. This is consistent with the small coordination number of Eu^{2+} ions in the amorphous system in contrast to the crystalline counterpart, as demonstrated by our previous x-ray absorption fine structure studies; in the case of $EuTiO_3$, for example, the coordination number of Eu^{2+} ions is reduced from 12 to about 6 upon amorphization, which increases the crystal-field strength for Eu^{2+}. Such variations of the local structure and electronic structure with amorphization are responsible for the enhancement of intra-atomic $4f$-$5d$ exchange interaction.

ACKNOWLEDGMENTS

The soft- and hard-x-ray experiments at the SPring-8 were performed with the approval of the JASRI (Proposals No. 2010B1704 and No. 2010B1729). This research was supported by Grants-in-Aid for Scientific Research on Priority Areas (Grant No. 474) and (B) (Grant No. 22360273) and Challenging Exploratory Research (Grant No. 23655198) from MEXT and for JSPS Fellows (Grant No. 22-1280) from JSPS.

*Corresponding author: fujita@dipole7.kuic.kyoto-u.ac.jp

[1] R. A. Verhelst, R. W. Kline, A. M. de Graaf, and H. O. Hooper, Phys. Rev. B **11**, 4427 (1975).
[2] A. Ito, E. Torikai, H. Yamauchi, and Y. Syono, J. Phys. C **15**, 2759 (1982).
[3] J. P. Sanchez, J. M. Friedt, R. Horne, and A. J. Van Duyneveldt, J. Phys. C **17**, 127 (1984).
[4] P. Beauvillain, C. Dupas, J. P. Renard, and P. Veillet, Phys. Rev. B **29**, 4086 (1984).
[5] J. L. Shaw, A. C. Wright, R. N. Sinclair, G. K. Marasinghe, D. Holland, M. R. Lees, and C. R. Scales, J. Non-Cryst. Solids **345&346**, 245 (2004).
[6] H. Akamatsu, K. Tanaka, K. Fujita, and S. Murai, Phys. Rev. B **74**, 012411 (2006).
[7] H. Akamatsu, S. Oku, K. Fujita, S. Murai, and K. Tanaka, Phys. Rev. B **80**, 134408 (2009).
[8] H. Akamatsu, J. Kawabata, K. Fujita, S. Murai, and K. Tanaka, Phys. Rev. B **84**, 144408 (2011).
[9] H. Akamatsu, K. Fujita, S. Murai, and K. Tanaka, Phys. Rev. B **81**, 014423 (2010).
[10] Y. Zong, K. Kugimiya, K. Fujita, H. Akamatsu, K. Hirao, and K. Tanaka, J. Non-Cryst. Solids **356**, 2389 (2010).
[11] H. Akamatsu, K. Fujita, Y. Zong, N. Takemoto, S. Murai, and K. Tanaka, Phys. Rev. B **82**, 224403 (2010).
[12] Y. Zong, K. Fujita, H. Akamatsu, S. Murai, and K. Tanaka, Phys. Status Solidi C **8**, 3051 (2011).
[13] T. R. McGuire, M. W. Shafer, R. J. Joenk, H. A. Alperin, and S. J. Pickart, J. Appl. Phys. **37**, 981 (1966).

[14]C. L. Chien, S. Debenedetti, and F. D. S. Barros, Phys. Rev. B **10**, 3913 (1974).
[15]J. E. Greedan and G. J. McCarthy, Mater. Res. Bull. **7**, 531 (1972).
[16]Y. Zong, K. Fujita, H. Akamatsu, S. Nakashima, S. Murai, and K. Tanaka, J. Am. Ceram. Soc. **95**, 716 (2012).
[17]T. Kasuya, IBM J. Res. Dev. **14**, 214 (1970).
[18]A. Mauger and C. Godart, Phys. Rep. **141**, 51 (1986).
[19]T. R. McGuire and M. W. Shafer, J. Appl. Phys. **35**, 984 (1964).
[20]G. van der Laan, B. T. Thole, G. A. Sawatzky, J. B. Goedkoop, J. C. Fuggle, J. M. Esteva, R. Karnatak, J. P. Remeika, and H. A. Dabkowska, Phys. Rev. B **34**, 6529 (1986).
[21]C. T. Chen, Y. U. Idzerda, H.-J. Lin, N. V. Smith, G. Meigs, E. Chaban, G. H. Ho, E. Pellegrin, and F. Sette, Phys. Rev. Lett. **75**, 152 (1995).
[22]B. T. Thole, G. van der Laan, J. C. Fuggle, G. A. Sawatzky, R. C. Karnatak, and J.-M. Esteva, Phys. Rev. B **32**, 5107 (1985).
[23]T. Kinoshita, H. P. N. J. Gunasekara, Y. Takata, S. Kimura, M. Okuno, Y. Haruyama, N. Kosugi, K. G. Nath, H. Wada, A. Mitsuda, M. Shiga, T. Okuda, A. Harasawa, H. Ogasawara, and A. Kotani, J. Phys. Soc. Jpn. **71**, 148 (2002).
[24]J. Holroyd, Y. U. Idzerda, and S. Stadler, J. Appl. Phys. **95**, 6571 (2004).
[25]V. V. Krishnamurthy, D. J. Keavney, D. Haskel, J. C. Lang, G. Srajer, B. C. Sales, D. G. Mandrus, and J. L. Robertson, Phys. Rev. B **79**, 014426 (2009).
[26]R. S. Selinsky, D. J. Keavney, M. J. Bierman, and S. Jin, Appl. Phys. Lett. **95**, 202501 (2009).
[27]Y. H. Matsuda, Z. W. Ouyang, H. Nojiri, T. Inami, K. Ohwada, M. Suzuki, N. Kawamura, A. Mitsuda, and H. Wada, Phys. Rev. Lett. **103**, 046402 (2009).
[28]B. J. Ruck, H. J. Trodahl, J. H. Richter, J. C. Cezar, F. Wilhelm, A. Rogalev, V. N. Antonov, Binh Do Le, and C. Meyer, Phys. Rev. B **83**, 174404 (2011).
[29]T. Nakamura, T. Hirono, T. Kinoshita, Y. Narumi, M. Hayashi, H. Nojiri, A. Mitsuda, H. Wada, K. Kodama, K. Kindo, and A. Kotani, J. Phys. Soc. Jpn. **81**, 103705 (2012).
[30]T. Nakamura, T. Muro, F. Z. Guo, T. Matsushita, T. Wakita, T. Hirono, Y. Takeuchi, and K. Kobayashi, J. Electron Spectrosc. Relat. Phenom. **144–147**, 1035 (2005).
[31]M. Suzuki, N. Kawamura, M. Mizumaki, A. Uerta, H. Maruyama, S. Goto, and T. Ishikawa, Jpn. J. Appl. Phys. **37**, L1488 (1998).
[32]M. W. Shafer and J. C. Suits, J. Am. Ceram. Soc. **49**, 261 (1966).
[33]K. Tanaka, K. Fujita, N. Soga, J. Qiu, and K. Hirao, J. Appl. Phys. **82**, 840 (1997).
[34]K. Tanaka, K. Fujita, N. Matsuoka, K. Hirao, and N. Soga, J. Mater. Res. **13**, 1989 (1998).
[35]H. Akamatsu, K. Fujita, Y. Nakatsuka, S. Murai, and K. Tanaka, Opt. Mater. (2012).
[36]K. Y. Ahn and J. C. Suits, IEEE Trans. Magn. **3**, 453 (1967).
[37]K. Y. Ahn and M. W. Shafer, J. Appl. Phys. **41**, 1260 (1970).
[38]T. Mitani, M. Ishibashi, and T. Koda, J. Phys. Soc. Jpn. **38**, 731 (1975).
[39]J. Ferre, B. Briat, C. Paparoditis, S. Pokrzywnicki, and R. Suryanarayanan, Solid State Commun. **11**, 1173 (1972).
[40]G. Güntherodt, J. Schoenes, and P. Wachter, J. Appl. Phys. **41**, 1083 (1970).
[41]J. C. Suits and B. E. Argyle, J. Appl. Phys. **36**, 1251 (1965).
[42]A. K. Zvezdin and V. A. Kotov, *Modern Magnetooptics and Magnetooptical Materials* (Taylor & Francis, London, 1997).
[43]C. Godart, J. C. Achard, G. Krill, and M. F. Ravet-Krill, J. Less-Common Met. **94**, 177 (1983).
[44]B. T. Thole, P. Carra, F. Sette, and G. van der Laan, Phys. Rev. Lett. **68**, 1943 (1992); P. Carra, B. T. Thole, M. Altarelli, and X. Wang, *ibid.* **70**, 694 (1993).
[45]S. P. Collins, D. Laundy, C. C. Tang, and G. van der Laan, J. Phys.: Condens. Matter **7**, 9325 (1995).